Effect of fracture voids on the swelling behaviour of Callovo-Oxfordian claystone

Feng Zhang, Yu-Jun Cui, Nathalie Conil, Jean Talandier

Effect of fracture voids on the swelling behaviour of Callovo-Oxfordian claystone

Feng Zhang[1], Yu-Jun Cui[1*], Nathalie Conil[2], Jean Talandier[2]

1: Ecole des Ponts ParisTech, Laboratoire Navier/CERMES, 6 et 8 avenue Blaise Pascal, 77455 Marne La Vallée cedex 2, France
2: CMHM, Andra, RD 960, 55290 Bure, France

***Corresponding author:**
Prof. Yu-Jun CUI
Ecole des Ponts ParisTech
6-8 av. Blaise Pascal, Cité Descartes, Champs-sur-Marne
77455 Marne-la-Vallée cedex 2
France

E-mail : yu-jun.cui@enpc.fr
Tel: + 33 1 64153550

Abstract: The Callovo-Oxfordian (COx) claystone has been considered as a possible host rock for deep geological repository of high-level radioactive waste in France. When constructing the repository, it is unavoidable to generate a fractured zone in the vicinity of excavated repository walls. In the assessment of the repository performance, it is important to investigate the role of the fractures on the swelling capacity of COx claystone and to further characterize the fractured zone evolution. In this study, the effect of fracture voids on the swelling behaviour of COx claystone was investigated by simulating the fracture voids with a space created by a limited amount of grains sandwiched between claystone disks, and by performing a series of swelling tests in oedometer under a low vertical stress (0.05 MPa) and swelling pressure tests under constant-volume condition. Results showed that, with water infiltrating into the sample with fracture voids, the grains collapsed before the swelling of claystone disks. The whole sample was composed of swelling zones corresponding to the claystone disks with higher dry density than the expected final value, and of compression zones corresponding to the initial fractures with lower dry density. Moreover, the axial strain and swelling pressure decreased as the fracture void increased. The maximum fracture voids that might be fully filled by the swelling of COx claystone (sealing) were found to be 5.14% - 7.65% without considering the long-term creep contribution in the field condition.

***Key words*:** COx claystone; Fracture voids; Swelling behaviour; Sealing

1 Introduction

The Callovo-Oxfordian (COx) claystone has been considered as a possible host rock for deep geological disposal of high-level radioactive waste by the French Radioactive Waste Management Agency (ANDRA) thanks to its favorable properties such as low permeability and diffusion coefficient, high retention capacity for radionuclides (ANDRA, 2005). In order to assess the reliability of the host rock as a geological barrier for radioactive waste confinement in field condition, an underground research laboratory (URL) was constructed at a depth of 490 m in the 150 m-thick formation of COx claystone in Bure, France (Armand et al., 2013). As excavation of the underground repository in this formation induced shear and tensile fractures, a damaged zone around the galleries was created with fractures smaller than 1 mm (Armand et al., 2014). A part of this zone is normally unsaturated during the construction and exploitation of the galleries due to ventilation. It becomes progressively saturated with the up-take of underground water. Under the effect of water infiltration, the COx claystone in the fractured zone is expected to swell and to close the excavation-induced fractures, leading to a significant reduction of water transmissivity. Thereby, in the assessment of repository performance, it is important to account for the swelling behaviour of the COx claystone with fractures.

The swelling behaviour of COx claystone under the effect of fractures has been scarcely reported in literature, mainly because of the difficulty related to the sampling of fractured samples in field (Armand et al., 2014), as well as the relatively large variability of natural COx claystone in terms of dry density and mineralogy (Conil et

al., 2018; Zhang et al., 2020). On the-other hand, the self-sealing behaviour of fractured COx claystone has been widely investigated by means of gas/water permeability tests in the laboratory and in the field condition (Davy et al., 2007; Zhang and Rothfuchs, 2008; Zhang, 2011; de La Vaissière et al., 2015; Auvray et al., 2017). It was found that the gas/water permeabilities of strongly fractured COx claystone sample significantly decreased after water re-saturation, indicating a relatively high self-sealing capacity of COx claystone. This point was confirmed by the X-ray tomography technique (Ando et al., 2017; Giot et al., 2018; Di Donna et al., 2019). Moreover, the swelling behavior of compacted sealing/backfilling materials in the presence of artificial fractures was also widely reported in literature (Wang et al., 2011, 2013; Bian et al., 2019; Jia et al., 2019). Results show that the swelling pressure decreased as the fractures increased. Basically, the sealing of fractured claystone is a complex long-term hydro-mechanical process, which is controlled by many factors such as the extent and intensity of fractures, the swelling capability of claystone as well as the boundary conditions (e.g., the stress state, the build-up backfill pressure). From a practical point of view, well understanding the swelling behaviour of COx claystone with the presence of fractures is helpful in analyzing the self-sealing process in the fractured zone.

In this study, a series of swelling tests were performed in oedometer on COx claystone with different fracture voids either under a low vertical stress (0.05 MPa) or under constant-volume condition, the fracture voids being simulated by a limited quantity of COx claystone grains of defined sizes, sandwiched between COx

claystone disks. For comparison and further analysis, the results from the swelling and compression tests performed by Zhang et al. (2020) on intact COx claystone samples were considered. After the tests under constant-volume condition, the water content and dry density profiles were determined, allowing further interpretation of the swelling behaviour of COx claystone samples with fracture voids. Emphasis was put on the initial fracture void on the swelling and swelling pressure as well as the maximum fracture voids that might be sealed by COx claystone swelling, which are key questions in the assessment of deep geological repository performance of nuclear waste disposal.

2 Materials and methods

2.1 Materials

Undisturbed COx claystone samples were extracted at 490 m depth from the Underground Research Laboratory (URL) at Bure in France, following the direction parallel to the bedding plane that was found to be parallel to the ground surface through observation of a piece of COx claystone immersed in water. They were then covered by foil and conserved in a fully confined cell (T1), preventing water loss and soil rebounding (Conil et al., 2018). At 490 m depth, the average mineralogical composition is (Armand et al., 2013): 50-55 % clay minerals, 20% tectosilicates, 20-25% carbonates and 3% other minerals (subordinate pyrite and iron oxides). The clay minerals composition contains 55% I/S (interstratified illite-smectite), 30% illite and 15% kaolinite and chlorite.

129 The synthetic water used in this study had the same chemical composition as the
130 pore water of COx claystone from the ANDRA URL in Bure (Table 1).
131
132 **2.2 Preparation of samples**
133 In this study, five cores (EST56054, EST56056, EST56062, EST57173 and
134 EST57175) with 300 mm length and 80 mm diameter were used. After opening the
135 COx claystone from the confined cell (T1) in the laboratory, a cylinder with 50 mm
136 diameter was drilled in the direction perpendicular to the bedding. Then, this cylinder
137 (50 mm diameter) was cut with a scroll saw machine to prepare disks with 5 mm
138 height for samples with fracture voids. The fracture voids for samples with two, three
139 and four disks were simulated with a defined space created by COx claystone grains
140 of defined sizes between the disks of 5 mm height each (see Fig. 1). The grains were
141 obtained by crushing intact COx claystone and passing through different sieves, and
142 their mass was kept less than 1% of the whole sample in order to minimize its effect
143 on the global swelling behaviour of the sample. The fracture void of the sample was
144 defined as the volume of fractures divided by the volume of the whole sample
145 (including the volume of disks and fractures).
146
147 **2.3 Experimental methods**
148 The swelling tests on the samples with fracture voids under 0.05 MPa vertical stress
149 were performed in a conventional oedometer. The inner surface of the metallic cell
150 was smeared with silicone grease in order to minimize the side friction during the
151 swelling tests, following ASTM D2435-96. The experimental programs are shown in

Table 2. Two tests were performed on samples with two disks (CS(2 disks)01-02), five tests on samples with three disks (CS(3 disks)01-05) and two tests on samples with four disks (CS(4 disks)01-02), the height of each disk being 5 mm. The crushed COx grains respectively passing through sieves of 0.2-0.25, 0.315-0.4, 0.5-0.63, 0.63-0.8 and 0.8-1.0 mm were used, allowing creation of the fracture voids ranging from 1.78% to 10.68% (see Table 2). Note that swelling tests under different vertical stresses (CS(1 disk)01-04) and compression test (SC(1 disk)01) on intact samples with a height of 10 mm (see Table 2) were performed by Zhang et al. (2020). To facilitate the sample installation in the oedometer cell, an initial small gap corresponding to a void ratio of 0.015 - 0.02 (see Table 2) was kept between the sample and the oedometer cell. In further analysis, these initial gaps are regarded as space allowing soil free swelling (Zhang et al., 2020). However, for the samples with fractures, due to the difficulty of calculating the void ratio corresponding to initial gaps, these initial gaps together with the fractures created by grains contributed to the initial fracture voids as well as the global void ratios. Moreover, the void ratio corresponding to the filter paper thickness (0.09 mm) was equal to 0.009. Thus, the effect of such small void ratio on the swelling behaviour during wetting was ignored. It is worth noting that to facilitate the synthetic water infiltration, the top, bottom and lateral surfaces of sample were covered with filter papers. With water infiltration from the bottom of the cell (the water head was about 0.5 m), water will go through the filter papers into the bottom, and then through the lateral filter paper to the fractures and the top surface, prior to the disks. Thereby, the adopted water infiltration

condition was close to the field condition: water mainly infiltrates into fractures prior to being adsorbed by claystone. The axial displacement was monitored using a LVDT (Linear Variable Differential Transformer), and the deformation was considered as stabilized when the axial strain rate was less than 5×10^{-4}/8 h (AFNOR, 1997).

The swelling pressure was determined by the constant-volume method, and the experimental setup is presented in Fig. 2. The sample covered with filter papers was placed between two porous stones in a stainless cell with a diameter of 50 mm. The synthetic water was infiltrated from the bottom of the cell and a force transducer was mounted to measure the axial force/swelling pressure. The experimental program is shown in Table 3. Three tests were performed on samples with two disks (CV(2 disks)01-03), two tests on samples with three disks (CV(3 disks)01-02) and one test on sample with four disks (CV(4 disks)01). The initial fracture voids varied from 2.44% to 7.65% (Table 3). Note that the swelling pressure test CV(1 disk)01 on intact sample with a height of 10 mm was performed by Zhang et al. (2020). When the swelling pressure was stabilized, the test was considered as completed (Villar and Lloret, 2004).

It is worth noting that the sealing of excavation-induced fractures (smaller than 1 mm) is a complex long-term hydro-mechanical process (Armand et al., 2014), which is controlled by many factors such as the extent and intensity of fractures, the swelling capability of claystone as well as the boundary conditions (e.g., the stress state). This is the reason why the different grain sizes (0.2-0.25 mm, 0.315-0.4 mm, 0.5-0.63 mm, 0.63-0.8 mm, 0.8-1.0 mm) and the different quantities of disks (2, 3 and 4), as well as

196 the two boundary conditions (constant-stress 0.05 MPa and constant-volume
197 condition) were considered in this study.

198 After the swelling tests under constant-volume condition, the samples were
199 extracted from the oedometer cell and then divided into several layers (see Fig. 1). For
200 the sample with two disks (Fig. 1a), layers 1, 2 included the top and bottom disks,
201 respectively, while layer 1.5 included the top and bottom disks, and the fracture voids
202 in between. Corresponding definitions were adopted for the samples with three and
203 four disks (Figs. 1b and 1c). Each layer was then cut into small pieces for the water
204 content and dry density determinations. The water content was determined by oven
205 drying the samples at 105℃ for 24 h and the dry density was determined by
206 immersing the samples into a non-wetting hydrocarbon liquid called Kerdane (Delage
207 et al., 2007; Tang et al., 2010, 2011; Zhang et al., 2018). Accordingly, the water
208 content and dry density profiles were determined following the definitions of layers
209 shown in Fig. 1.

210 All the tests were performed at a controlled temperature of 20 ± 1°C.

211

212 ## 3 Experimental results

213 Fig. 3 shows the results from tests CS(1 disk)01-04 on intact samples (Zhang et al.,
214 2020). It can be observed that the axial strain slowly increased in the first 0.001 day
215 (1.4 min), then quickly increased till approximately 0.3 day (432 min). Afterwards,
216 the axial strain slowly increased until stabilization. In addition, the stabilized axial
217 strain decreased with the increase of vertical stress.

Fig. 4a presents the compression curve from test SC(1 disk)01 on intact sample (Zhang et al., 2020). It appeared that, upon wetting, the sample swelled under a low vertical stress of 0.05 MPa. After the swell completion, further compression gave a normal consolidation curve (NCL) that allowed determination of the compression index in the range of stress from 2 to 16 MPa (C_c = 0.0366). In addition, by approximating each curve with two straight lines, the yield stress σ'_y was determined, equal to 0.55 MPa, as indicated by the arrow in this figure. For further analysis, the compression curve shown in Fig. 4a was used to determine the oedometric modulus E_{oed} as follows:

$$E_{oed} = -\frac{d\sigma_v}{d\varepsilon_v} = -h_i \frac{d\sigma_v}{dh} = -(1+e_0)\frac{d\sigma_v}{de} \quad (1)$$

where h_i and e_0 are respectively the initial height and void ratio of the sample, $d\varepsilon_v$, dh and de are respectively the volumetric strain, height and void ratio changes under an increment of vertical stress $d\sigma_v$. Fig. 4b plots the E_{oed} versus vertical stress in a logarithmic scale. It appeared that, upon loading below 0.5 MPa stress (close to the yield stress 0.55 MPa), the E_{oed} decreased as the vertical stress increased. By contrast, beyond the yield stress 0.55 MPa, the E_{oed} linearly increased. This is consistent with the results reported by Nguyen et al. (2013) on Boom clay and by Ye et al. (2014) on GMZ01 bentonite: with the increase of vertical stress, the E_{oed} decreased at the beginning and then linearly increased when the stress was higher than the yield stress in a logarithmic scale. These observations suggest that the E_{oed} is a good indicator of soil yielding. Moreover, a linear relationship between the oedometric modulus and the vertical stress was obtained after yield.

The results from tests CS(2 disks)01-02 on samples with fracture voids are shown in Fig. 5 in terms of axial strain versus time (Fig. 5a) and void ratio versus time (Fig. 5b). For comparison, the result from test CS(1 disk)01 on intact sample (Zhang et al., 2020) was also presented. It is worth noting that when the axial strain was positive, the decrease/increase of axial strain referred to the decrease/increase of the magnitude. By contrast, in case of negative value, the decrease/increase of axial strain referred to the increase/decrease of the magnitude. It appeared from Fig. 5a that, for the intact sample (CS(1 disk)01), the axial strain increased with time until stabilization. For samples with fracture voids (tests CS(2 disks)01-02), the axial strain decreased in the first 0.001 day (1.4 min), showing a closing trend of fractures due to collapse of COx claystone grains. Afterwards, the axial strain slowly increased up to approximately 0.006 day (8.6 min), then quickly increased till 0.3 day (432 min). Finally, the axial strain slowly increased until stabilization. Moreover, the higher the initial fracture void, the larger the initial collapse and the smaller the final axial strain at stabilization, suggesting the significant effect of fracture voids. The results identified in Fig. 5b show that, for intact sample, the void ratio increased all the time, while for samples with fracture voids, the void ratio decreased in the first 0.001 day (1.4 min), then increased until stabilization. Moreover, the higher the initial fracture void, the larger the final void ratio at stabilization. The results from tests CS(3 disks)01-05 and tests CS(4 disks)01-02 on samples with fracture voids are presented in Fig. 6 and Fig. 7, respectively. For comparison, the result from test CS(1 disk)01 on intact sample (Zhang et al., 2020) was also presented. As for samples with two disks

262 shown in Fig. 5, it is observed that: i) for samples with fracture voids, the axial strain
263 (or void ratio) decreased during the initial collapse stage, then increased until
264 stabilization; ii) the higher the initial fracture void, the larger the final void ratio and
265 the smaller the final axial strain at stabilization.

266 The maximum void that could be filled by claystone swelling corresponded to
267 the one at which the total swelling part was equal to the total collapse part. For its
268 determination, all the axial strains corresponding to the total collapse and swelling
269 parts, as well as the total axial strains were determined from the curves of axial strain
270 versus time shown in Figs. 5a, 6a and 7a. Taking test CS(2 disks)01 as an example
271 (see Fig. 5a): i) during hydration, water flowed into the fracture voids, leading to a
272 collapse of grains up to -0.84% at approximately 0.001 day (1.4 min); ii) the total
273 axial strain at stabilization being 1.29%, the axial strain related to the total swelling of
274 disks was thus calculated to be 2.13% (equal to 1.29% - (-0.84%)). For other tests
275 (CS(2 disks)02, CS(3 disks)01-05 and CS(4 disks)01-02), the total axial strains and
276 the corresponding collapse and swelling parts were determined in the same manner,
277 and the results are presented in Fig. 8. It appeared that, with increasing initial fracture
278 void, the total axial strain and the collapse part significantly decreased, while the
279 swelling part slightly decreased, revealing the significant effect of fracture voids. In
280 addition, the fracture void at which the swelling part was equal to the collapse part
281 (also zero total axial strain) could be also determined from Fig. 8. Due to the scatter of
282 the test data, it appeared necessary to introduce two curves to define the upper and
283 lower limits for the total axial strain, as indicated in Fig. 8. The maximum fracture

voids that could be filled by the swelling of disks were thus estimated at 5.14%-7.65%. This suggests that only the fracture voids smaller than 5.14%-7.65% can be sealed by claystone swelling. The range of this maximum fracture void implies the variability of claystone in terms of mineralogy and dry density (Conil et al., 2018; Zhang et al., 2020). It should be however noted that this conclusion does not consider the long-term creep contribution in the field condition.

Fig. 9 shows the results from tests CV(1 disk)01, CV(2 disks)01-03, CV(3 disks)01-02 and CV(4 disks)01. It was observed that, for the intact sample (CV(1 disk)01) (Zhang et al., 2020), the swelling pressure first slowly then quickly increased. Afterwards, the swelling pressure slowly increased until stabilization. For the samples with fracture voids, the swelling pressure decreased in the first 0.001 day (1.4 min), showing a collapse feature. Afterwards, the swelling pressure slowly increased up to approximately 0.006 day (8.6 min), then quickly increased up to 0.3 day (432 min). Finally, the swelling pressure slowly increased until stabilization. Moreover, the stabilized swelling pressure decreased as the initial fracture void increased, suggesting a significant effect of fracture voids (Wang et al., 2011, 2013).

Figs. 10a-10f present the water content and dry density profiles (following the definitions of layers in Fig. 1) of samples with fracture voids wetted under constant-volume condition. For comparison, the expected final dry densities here calculated using the total mass of COx solids (including the disks and the grains) divided by the volume of the whole sample at the end of the test (including the disks and the fracture voids) were also presented. It appeared that, for samples with two

disks (Figs. 10a-10b), larger water contents and lower dry densities were found at position 1.5 that included the top and bottom disks as well as the fracture void in between, as compared with the values at position 1 (top disk) and position 2 (bottom disk). In addition, with increasing initial fracture void, the water contents for positions 1, 1.5 and 2 increased, while the dry densities for positions 1 and 2 decreased. Moreover, the measured dry densities for disks (represented by the full numbers 1 and 2) were larger than the expected final one, showing the significant effect of fracture voids. The similar phenomena were observed for samples with three and four disks (Figs. 10c-10f): i) larger water contents and lower dry density were found for disks sandwiching fracture voids, as compared with the values for disks only; ii) with increasing initial fracture void, the water contents for disks, and for disks sandwiching fracture voids increased, while the corresponding dry densities decreased; iii) the measured dry density of disks were larger than the expected final one.

4 Discussion

During the hydration of sample with fracture voids, the synthetic water flowed into the fracture voids first. As a result, the grains were fully hydrated and subsequently collapsed, leading to a decrease of axial strain and swelling pressure before 0.001 day (1.4 min), as shown in Figs. 5, 6, 7 and 9. Afterwards, the disks started to swell (after 0.001 day (1.4 min) in Figs. 5, 6, 7 and 9), and the sample showed swelling (at which the sample with a dry density larger than the expected final state, was subjected to further swelling with a decrease of dry density over time) and compression zones

328 (where the sample with a dry density lower than the expected final state, was
329 subjected to compression with an increase of dry density over time), in agreement
330 with test results on MX80 bentonite by Bian et al. (2019). Examination of the dry
331 density profiles in Figs. 10b, 10d and 10f showed that the disks corresponded to the
332 swelling zones, while the initial fracture voids corresponded to the compression zones.
333 Thereby, the decrease of axial strain of swelling part with initial fracture void
334 identified in Fig. 8 represented the compression of grains by the swelling of disks.
335 The larger the initial fracture void, the larger the compression of swollen grains. This
336 explained the decrease of the total axial strain (Fig. 8) and the swelling pressure (Fig.
337 9) with the increase of initial fracture void.

338 For further analysis, all the results of samples with fracture voids under
339 constant-volume condition were replotted in Fig. 11 in terms of the measured swelling
340 pressure versus the expected final void ratio. The expected final void ratio was
341 calculated using the total volume of voids (including the voids in the disks and
342 fracture voids) divided by the total volume of solids (including the solids in the disks
343 and grains). For comparison, the evolution of swelling pressure with the void ratio of
344 intact COx claystone samples (tests CS(1 disk)01-04 listed in Table 2 and CV(1
345 disk)01 listed in Table 3) is also presented. It is worth noting that the swelling line
346 determined by the swelling tests on intact COx claystone samples defined the swelling
347 limit: the samples upon wetting from the same initial state stopped at this limit,
348 whatever the stress path followed (Zhang et al., 2020). It appeared that at the same
349 swelling pressure, higher void ratio was found for the samples with fracture voids.

This might be due to the fracture voids that were not fully filled at stabilization of swelling. This deduction was confirmed by the swollen grain distributions on the surface of disk after test CV(3 disks)02 (see Fig. 12, obtained by camera): the swollen grains distributed in an inhomogeneous fashion and the inter-grain voids could be clearly identified, indicating that the initial fracture voids created by grains were not fully filled. If the void ratio corresponding to the fracture voids that were not filled was subtracted from the global void ratio, the relationship between the swelling pressure and the void ratio was expected to be similar to that for intact samples. To verify this point, the variation of swelling pressure with the average void ratio of disks (average value of disks calculated from the dry density values after the tests shown in Table 3) were considered and the results are presented in Fig. 13. It appeared that at the same swelling pressure, the void ratios of disks were close to those on the swelling line, confirming that the difference identified in Fig. 11 was due to the fracture voids which were not fully filled. In that case, the transmission of total swelling pressure in the fracture voids zone was controlled by the swollen grains. It is worth noting that the slightly higher void ratio of disks observed in Fig. 13 could be partly attributed to the rebound while extracting the samples from the oedometer cell. It could be also due to the natural material variability in terms of mineralogy and dry density (Conil et al., 2018; Zhang et al., 2020).

For further analyzing the compression of swollen grains under constant-volume condition, the oedometric modulus E_{oed} defined in Eq. (1) was considered. As mentioned previously, the void ratio of grain was not measured after the swelling test,

which rendered the calculation of oedometric modulus E_{oed} of grain by Eq. (1) difficult. Note however that the compression of swollen grains approximately corresponded to the swelling of disks under constant-volume condition: i) the swelling pressure generated by the disks' swelling was approximately equal to the value that was imposed to the grains' compression; ii) the corresponding axial displacement of the disks' swelling was equal to that of the grains' compression. Moreover, the void ratios of the disks and grains before hydration were also the same, equal to the initial value e_0. Thus, the oedometric modulus E_{oed} of grains was approximately equal to the value of disks for simplicity. Taking test CV(2 disks)01 as an example, the oedometric modulus E_{oed} of grains was determined as follows: i) the swelling pressure at the start of disks' swelling and the corresponding void ratio were firstly determined. With water infiltration, the grains collapsed and the swelling pressure quickly decreased from the initial stress of 0.059 MPa to the lowest value of 0.0389 MPa at approximately 0.001 day (1.4 min) (Fig. 9), where the disks could reasonably be regarded to start to swell and the corresponding void ratio was determined (0.2098, average value of top and bottom disks calculated from the dry density before the test); ii) the swelling pressure at stabilization and the corresponding void ratio of disks were determined afterwards. The stabilized swelling pressure was 0.346 MPa, and the corresponding void ratio of disks was determined (0.2533, average value of top and bottom disks calculated from dry density after the test in Table 3); iii) the E_{oed} corresponding to the swelling of disks was finally calculated ((0.346 MPa - 0.0389 MPa) × (1 + 0.2098) / (0.2533 - 0.2098) = 8.54 MPa). Thus, the

394 E_{oed} of grains under 0.346 MPa stress was estimated at 8.54 MPa. For other tests
395 (CV(2 disks)02-03, CV(3 disks)01-02 and CV(4 disks)01), the E_{oed} of grains was
396 estimated in the same manner, and the results are shown in Fig. 14. For comparison,
397 the results of E_{oed} that was determined from oedometer test shown in Fig. 4b are also
398 presented. It appeared that: i) the E_{oed} of grains was lower than that of intact sample; ii)
399 the E_{oed} of grains was lower than that deduced from the normally consolidated line
400 (NCL). This could be attributed to the fracture voids that were not fully filled (Fig.
401 12), which did not enable the compression of swollen grains to obey the
402 one-dimensional K_0 condition. It could be logically deduced that the E_{oed} of grains
403 would be closer to that deduced from NCL if the quantity of grains or the stress
404 during hydration increased. Following up this logic, the line of E_{oed} versus vertical
405 stress was extrapolated to the NCL. A stress 1.56 MPa was obtained at the intersection
406 of the two lines. This stress corresponds to the value which theoretically verifies the
407 one-dimensional K_0 compression. In that case, the fracture voids are expected to be
408 totally filled.
409

410 # 5 Conclusions

411 In this study, the effect of fracture voids on the swelling behaviour of COx claystone
412 was experimentally investigated by performing swelling tests either under 0.05 MPa
413 vertical stress or under constant-volume condition. At the end of swelling tests under
414 constant-volume condition, the water content and dry density profiles were
415 determined. The results obtained allow the following conclusions to be drawn.

During the hydration of COx claystone samples with fracture voids, the grains collapsed first while in contact with water. Afterwards, the disks started to swell and the whole sample presented swelling zones corresponding to the claystone disks and compression zones corresponding to the initial fracture voids.

The axial swelling strain and swelling pressure decreased as the initial fracture void increased. The correlation between the swelling pressure for sample with fracture voids and the expected final void ratio was found to be higher than that of intact sample, which was explained by the fact that the fracture voids were not fully filled.

The maximum fracture voids that might be fully filled or sealed by the swelling of COx claystone were found to be 5.14% - 7.65% without considering the long-term creep contribution in the field condition.

References

AFNOR, 1997. Sols: reconnaissance et essais. Essais oedométriques. Partie 1: Essai de compressibilité sur matériaux fins quasi saturés avec chargement par paliers.

ANDRA, 2005. Synthesis - evaluation of the feasibility of a geological repository in anargillaceous formation. France, ANDRA.

Ando, E., Desrues, J., Charrier, P., Bésuelle, P., Kanso, S., Salager, S., 2017. Analysis of COX self sealing behaviour from x-ray computed tomography images. Séminaire ANDRA, Chatenay-Malabry, France.

ASTM, 1996. Standard Test Method for One-Dimensional Consolidation Properties of Soils. D2435-96.

Armand, G., Noiret, A., Zghondi, J., Seyedi, D.M., 2013. Short- and long-term behaviors of drifts in the Callovo-Oxfordian claystone at the Meuse/Haute-Marne Undergroud Research Laboratory. J. Rock Mech. Geotech. Eng. 5, 221-230.

Armand, G., Leveau, F., Nussbaum, C., De La Vaissière, R., Noiret, A., Jaeggi, D., Landrein, P., Righini, C., 2014. Geometry and properties of the excavation-induced fractures at the Meuse/Haute-Marne URL drifts, Rock Mech. Rock Eng. 47(1), 21-41.

Auvray, C., Morlot, C., Giot, R., Demeurie, C., Talandier, J., 2017. Self-sealing of claystone under x-ray nanotomography: a newly-developed triaxial compression

cell. 3rd International Conference on Tomography of Materials and Structures Lund, Sweden, 26-30.
Bian, X., Cui, Y.J., Li, X.Z., 2019. Voids effect on the swelling behaviour of compacted bentonite. Géotechnique 69(7), 593-605.
Conil, N., Talandier, J., Djizanne, H., de La Vaissière, R., Righini-Waz, C., Auvray C, Morlot, C., Armand, G., 2018. How rock samples can be representative of in situ condition: A case study of Callovo-Oxfordian claystone. J. Rock Mech. Geotech Eng. 10, 613-623.
Davy, C.A., Skoczylas, F., Barnichon, J.D., Lebon, P., 2007. Permeability of macro-cracked argillite under confinement: gas and water testing. Phys. Chem. Earth 32, 667-680.
Delage, P., Le, T.T., Tang, A.M., Cui, Y.J., Li, X.L., 2007. Suction and in-situ stresses of deep Boom clay samples. Géotechnique. 57(1), 239-244.
Di Donna, A., Charrier, P., Salager, S., Bésuelle, P., 2019. Self-sealing capacity of argillite samples. E3S Web of Conferences 92, 03005.
Giot, R., Auvray, C., Talandier, J., 2018. Self-sealing of claystone under X-ray nanotomography. Geological Society, London, Special Publications, 482.
Jia, L.Y., Chen, Y.G., Ye, W.M., Cui, Y.J., 2019. Effects of a simulated gap on anisotropic swelling pressure of compacted GMZ bentonite. Eng. Geol. 248, 155-163.
de La Vaissière, R., Armand, G., Talandier, J., 2015. Gas and water flow in an excavation-induced fracture network around an underground drift : A case study for a radioactive waste repository in clay rock. J. Hydrol. 521, 141-156.
Nguyen, X.P., Cui, Y.J., Tang, A.M., Deng, Y.F., Li, X.L., Wouters, L., 2013. Effects of pore water chemical composition on the hydro-mechanical behavior of natural stiff clays. Eng. Geol. 166, 52-64.
Tang, C.S., Cui, Y.J., Tang, A.M., Shi, B., 2010. Experiment evidence on the temperature dependence of desiccation cracking behavior of clayey soils. Eng. Geol. 114(3-4), 261-266.
Tang, C.S., Cui, Y.J., Shi, B., Tang, A.M., Liu, C., 2011. Desiccation and cracking behaviour of clay layer from slurry state under wetting-drying cycles. Geoderma 166(1), 111-118.
Villar, M.V., Lloret, A., 2004. Influence of temperature on the hydro-mechanical behaviourof a compacted bentonite. Appl. Clay Sci. 26, 337-350.
Wang, Q., Tang, A.M., Cui, Y.J., Delage, P., Gatmiri, B., 2011. Experimental study on the swelling behaviour of bentonite/claystone mixture. Eng. Geol. 124, 59-66.
Wang, Q., Tang, A.M., Cui, Y.J., Delage, P., Barnichon, J.D., Ye, W.M., 2013. The effects of technological voids on the hydro-mechanical behaviour of compacted bentonite-sand mixture. Soil. Found. 53(2), 232-245.
Ye, W.M., Zhang, F., Chen, B., Chen, Y.G., Wang, Q., Cui, Y.J., 2014. Effects of salt solutions on the hydro-mechanical behavior of compacted GMZ01 bentonite. Environ. Earth Sci. 72, 2621-2630.
Zhang, C.L., Rothfuchs, T., 2008. Damage and sealing of clay rocks detected by measurements of gas permeability. Phys. Chem. Earth 33, S363-373.

Zhang, C.L., 2011. Experimental evidence for self-sealing of fractures in claystone. Phys. Chem. Earth 36, 1972-1980.

Zhang, F., Cui, Y.J., Zeng, L.L., Robinet, J.C., Conil, N., 2018. Effect of degree of saturation on the unconfined compressive strength of natural stiff clays with consideration of air entry value. Eng. Geol. 237, 140-148.

Zhang, F., Cui, Y.J., Conil, N., Talandier, J., 2020. Assessment of swelling pressure determination methods with intact Callovo-Oxfordian claystone. Rock Mech. Rock Eng. 53, 1879-1888.

List of Tables

List of Figures

Table 1 Salts used for synthetic water preparation

Salt	NaCl	$NaHCO_3$	KCl	$CaSO_4.2H_2O$	$MgSO_4.7H_2O$	$CaCl_2.2H_2O$	Na_2SO_4
Concentration (g/l)	1.950	0.130	0.035	0.630	1.020	0.080	0.700

Table 2 Test program for samples wetted under constant-stress condition and compression test

No.	Core	Initial void ratio with/without considering gap (void ratio corresponding to initial gap)	Initial water content (%)	Grain size (mm)	Initial fracture void (%)	Description
CS(1 disk)01	EST56062	0.217/0.202 (0.015)	6.61	-	-	Wetted under 0.05 MPa
CS(1 disk)02	EST56054	0.218/0.198 (0.02)	6.59	-	-	Wetted under 0.5 MPa
CS(1 disk)03	EST56054	0.220/0.202 (0.018)	6.59	-	-	Wetted under 2.0 MPa
CS(1 disk)04	EST56062	0.215/0.199 (0.016)	6.61	-	-	Wetted under 8.0 MPa
SC(1 disk)01	EST56062	0.217/0.202 (0.015)	6.61	-	-	Wetted under 0.05 MPa then load to 32 MPa
CS(2 disks)01	EST56062	-	6.61	0.5-0.63	3.16	Wetted under 0.05 MPa
CS(2 disks)02	EST57175	-	7.43	0.8-1.0	6.95	
CS(3 disks)01	EST56062	-	6.61	0.2-0.25	1.78	
CS(3 disks)02	EST56062	-	6.61	0.315-0.4	2.69	
CS(3 disks)03	EST57173	-	6.93	0.5-0.63	4.85	
CS(3 disks)04	EST57173	-	6.93	0.63-0.8	8.47	
CS(3 disks)05	EST57175	-	7.43	0.8-1.0	9.41	
CS(4 disks)01	EST57173	-	6.93	0.5-0.63	5.48	
CS(4 disks)02	EST57175	-	7.43	0.8-1.0	10.68	

Table 3 Test program for samples wetted under constant-volume condition

No.	Core	Grain size (mm)	Initial fracture void (%)	Water content before/after test (%)	Dry density before/after test (Mg/m^3)
CV(1 disk)01	EST56056	-	-	6.53/9.46	2.231/2.163
CV(2 disks)01	EST57173	0.315-0.4	2.44	6.93/10.08 (1) -/10.87 (1.5) 6.93/10.46 (2)	2.240/2.162 (1) -/2.106 (1.5) 2.224/2.146 (2)
CV(2 disks)02	EST57173	0.5-0.63	4.30	6.93/10.55 (1) 6.93/10.49 (2)	2.226/2.134 (1) 2.237/2.163 (2)
CV(2 disks)03	EST57173	0.63-0.8	5.66	6.93/10.97 (1) -/12.04 (1.5) 6.93/11.10 (2)	2.219/2.127 (1) -/-(1.5) 2.263/2.131 (2)
CV(3 disks)01	EST57175	0.5-0.63	6.11	7.43/10.75 (1) 7.43/10.64 (2) 7.43/10.74 (3)	2.227/2.121 (1) 2.218/2.145 (2) -/2.121 (3)
CV(3 disks)02	EST57173	0.63-0.8	7.65	6.93/10.85 (1) 6.93/11.12 (2) 6.93/11.02 (3)	2.244/2.126 (1) 2.230/2.113 (2) 2.256/2.114 (3)
CV(4 disks)01	EST57175	0.5-0.63	6.90	7.43/10.15 (1) -/10.53 (1.5) 7.43/10.45 (2) 7.43/10.56 (3) -/10.68 (3.5) 7.43/10.37 (4)	2.240/2.144 (1) -/2.124 (1.5) 2.230/2.136 (2) 2.243/2.132 (3) -/2.118 (3.5) 2.228/2.138 (4)

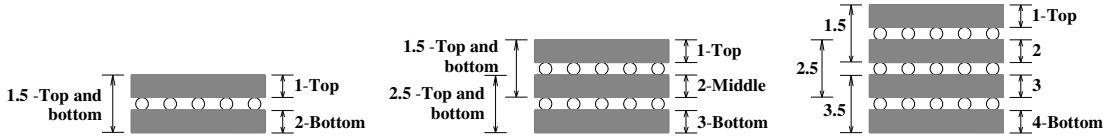

(a) two disks (b) three disks (c) four disks

Fig. 1. Schematic diagram of samples with fracture voids: (a) two disks, (b) three disks, (c) four disks

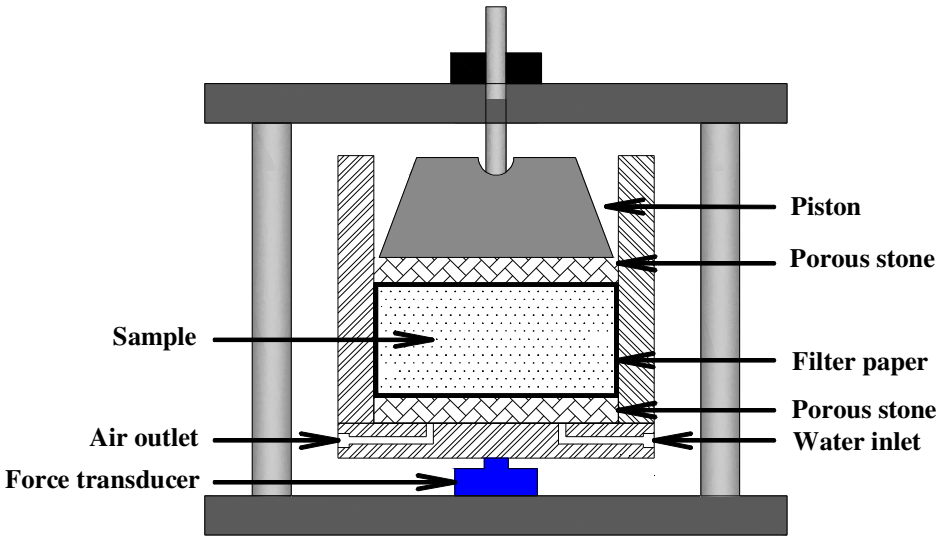

Fig. 2. Layout of the constant-volume cell

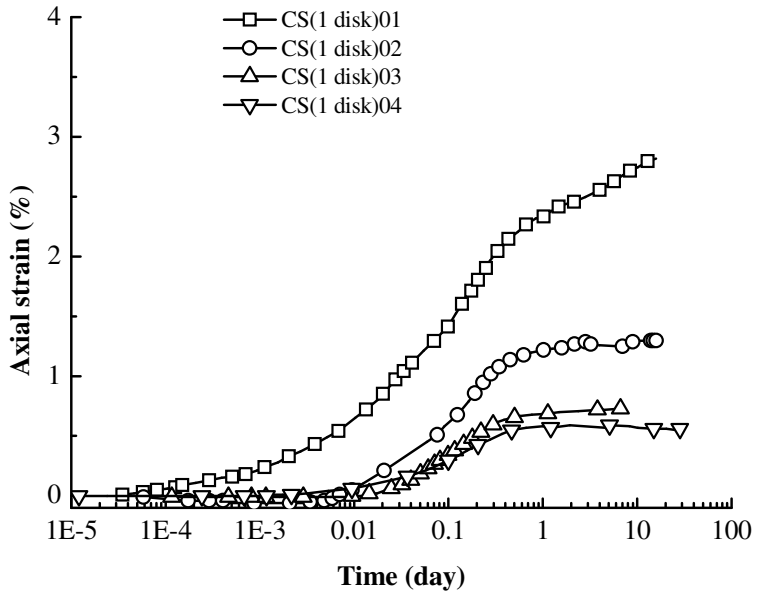

Fig. 3. Axial strain versus time for intact samples

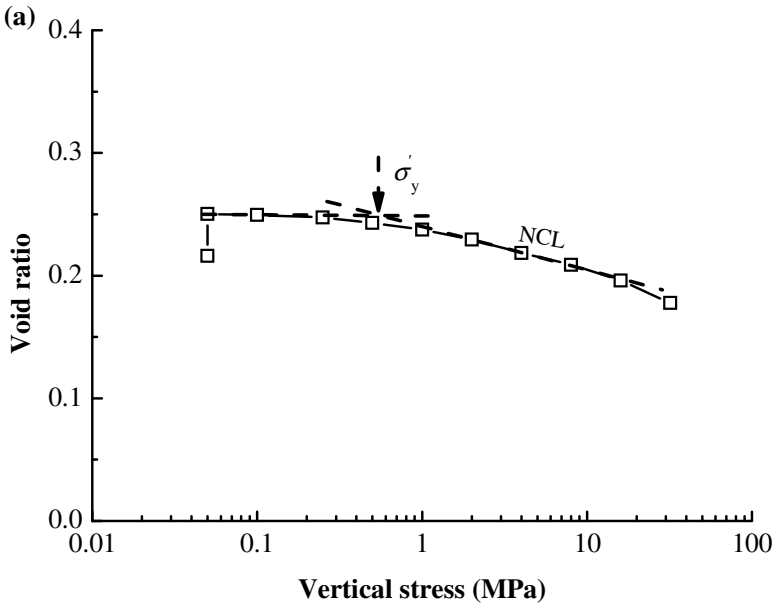

583

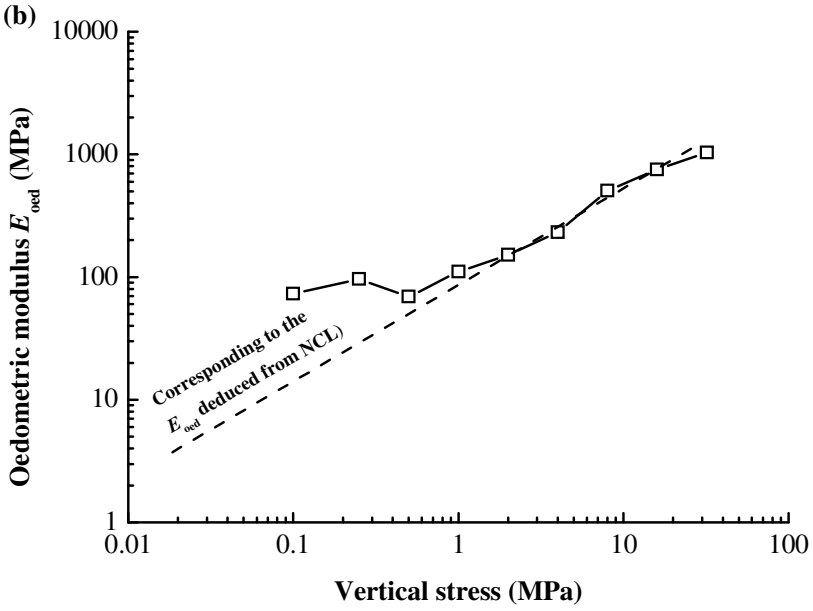

584

585 Fig. 4. Compression test SC(1 disk)01 on intact sample: (a) void ratio versus vertical stress, (b)
586 oedometric modulus versus vertical stress

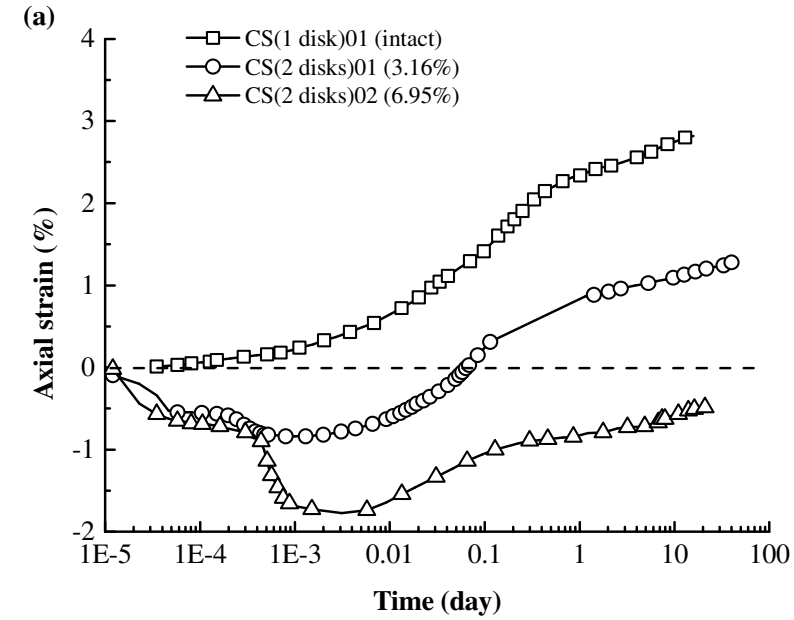

587

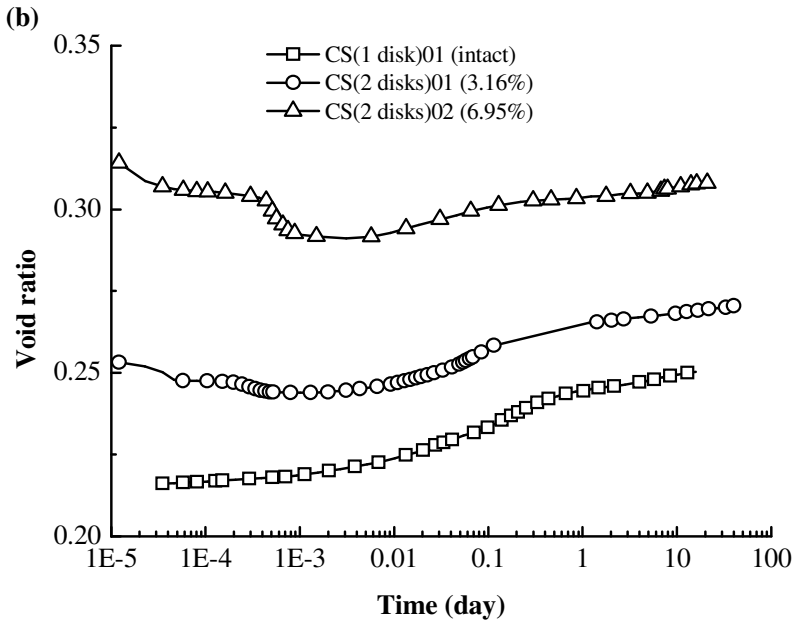

588

589 Fig. 5. Results of samples with fracture voids wetted under 0.05 MPa from tests CS(2 disks)01-02,
590 together with those of intact sample from test CS(1 disk)01: (a) axial strain, (b) void ratio

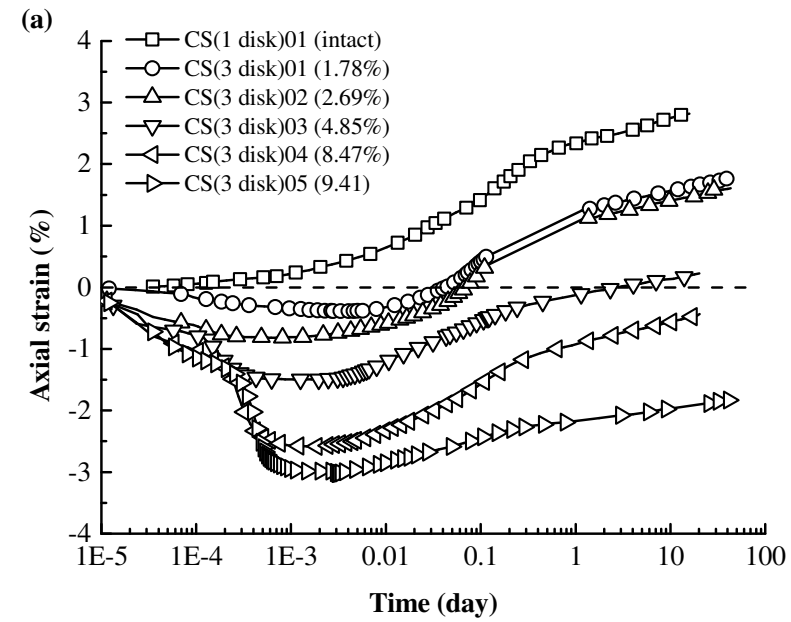

591

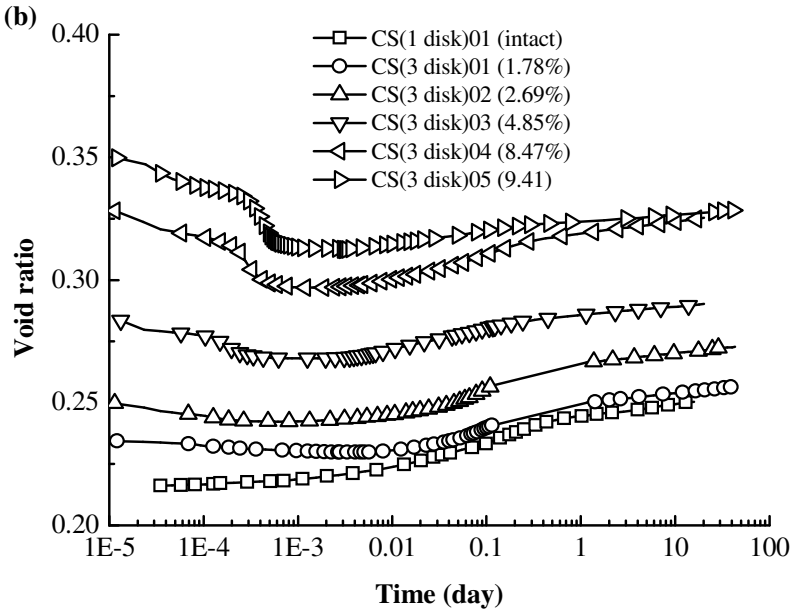

592

593 Fig. 6. Results of samples with fracture voids wetted under 0.05 MPa from tests CS(3 disks)01-05,
594 together with those of intact sample from test CS(1 disk)01: (a) axial strain, (b) void ratio

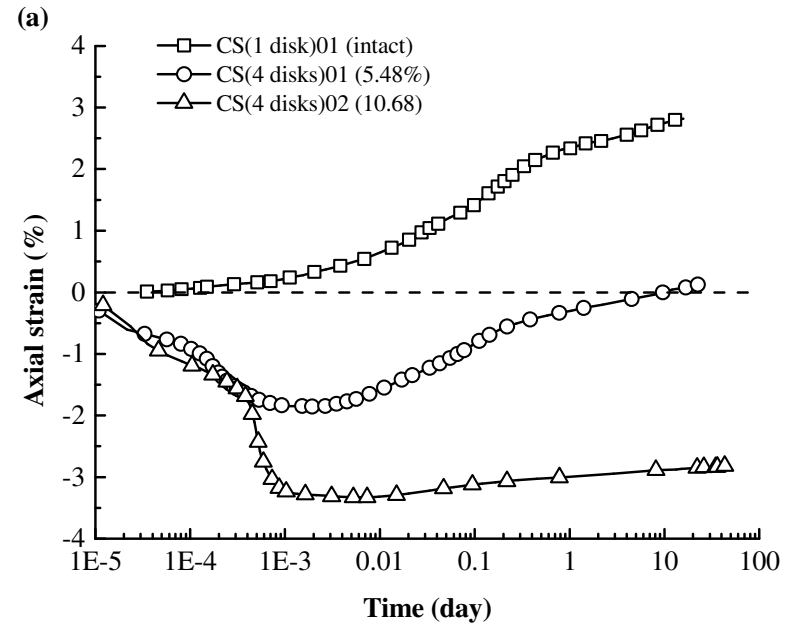

595

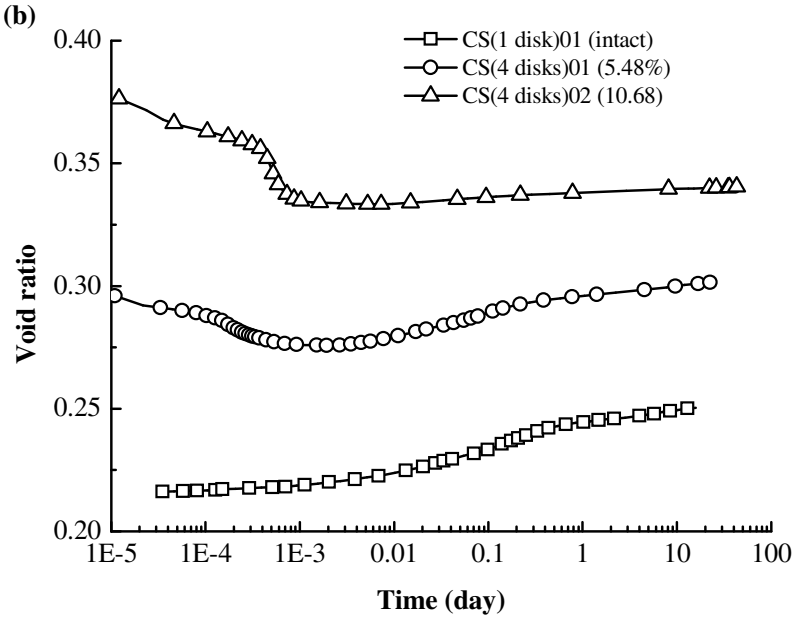

596

597 Fig. 7. Results of samples with fracture voids wetted under 0.05 MPa from tests CS(4 disks)01-02,
598 together with those of intact sample from test CS(1 disk)01: (a) axial strain, (b) void ratio

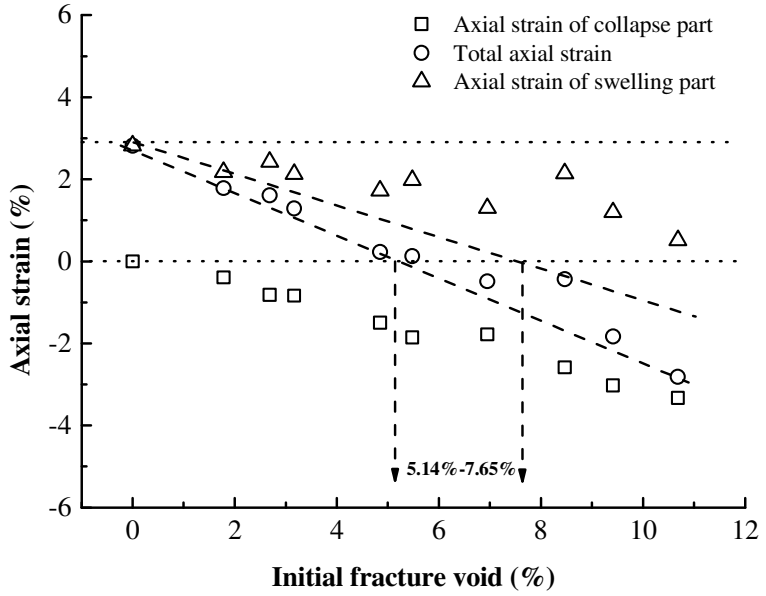

599

600 Fig. 8. Total axial strains and the corresponding collapse and swelling parts versus initial fracture
601 void for samples with one, two, three and four disks

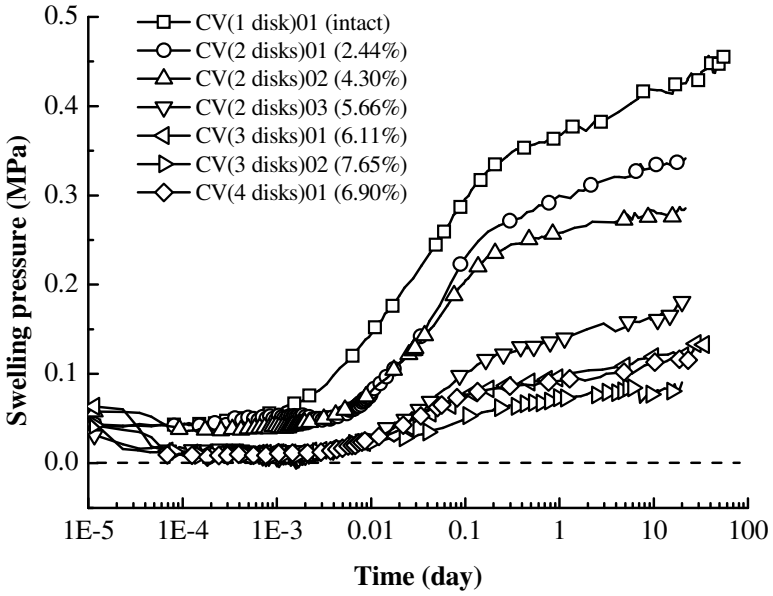

602

603 Fig. 9. Evolution of swelling pressure under constant-volume condition

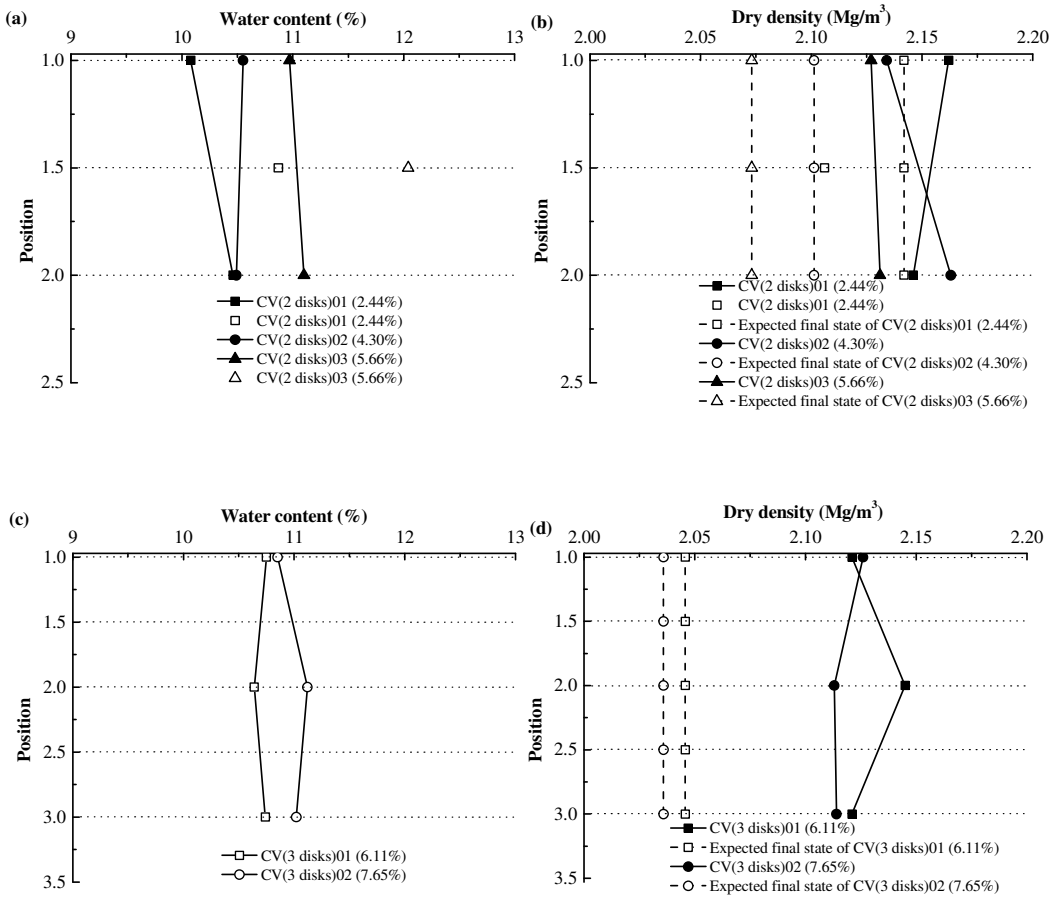

Fig. 10. Water content and dry density profiles for samples with fracture voids after swelling tests under constant-volume condition: (a) water content profile (two disks), (b) dry density profile (two disks), (c) water content profile (three disks), (d) dry density profile (three disks), (e) water content profile (four disks), (f) dry density profile (four disks)

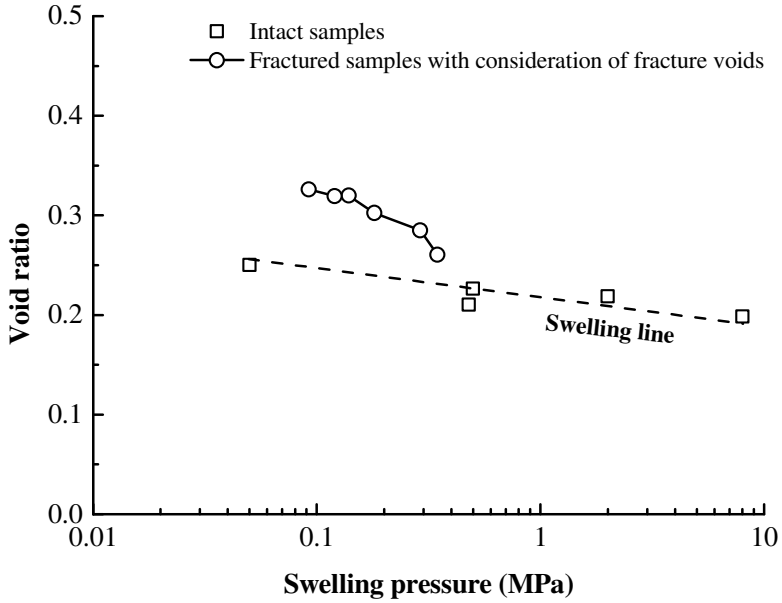

611

612 Fig. 11. Comparison of swelling pressure between intact samples and fractured samples with
613 consideration of fracture voids

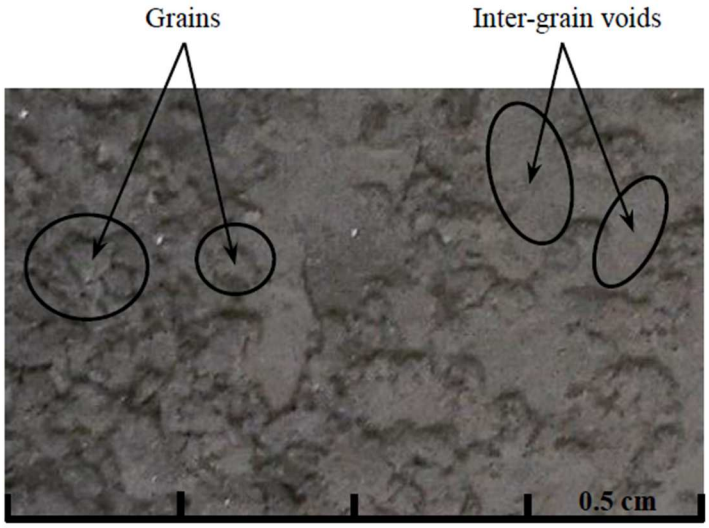

614

615 Fig. 12. Distribution of grains on the disk surface after test CV(3 disks)02

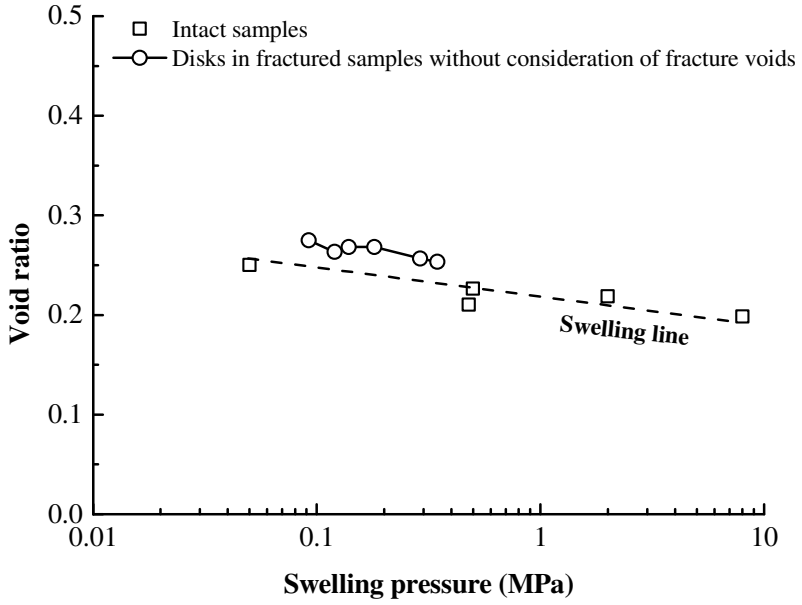

Fig. 13. Comparison of swelling pressure between intact samples and disks in fractured samples without consideration of fracture voids

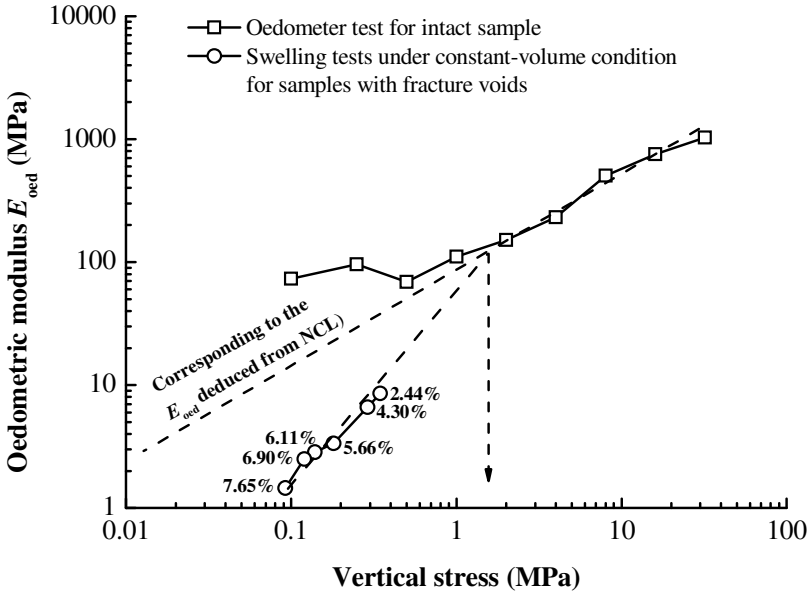

Fig. 14. Variation of oedometric modulus with vertical stress